Letter Vol. 44, No. 1 / 1 January 2019 / Optics Letters 77

Inverse-designed low-loss and wideband polarization-insensitive silicon waveguide crossing

Zejie Yu,† Aosong Feng,† Xiang Xi, and Xiankai Sun*

Department of Electronic Engineering, The Chinese University of Hong Kong, Shatin, New Territories, Hong Kong
**Corresponding author: xksun@cuhk.edu.hk*

Received 4 October 2018; revised 15 November 2018; accepted 15 November 2018; posted 16 November 2018 (Doc. ID 347492); published 20 December 2018

Waveguide crossings are an essential component for constructing complex and functional on-chip photonic networks. Polarization-insensitive waveguide crossings are desired because photonic networks usually involve light with different polarizations. Here, we propose a polarization-insensitive waveguide crossing on a 250-nm silicon-on-insulator platform by using an inverse design method. In simulation, the designed waveguide crossing can maintain insertion loss below 0.18 (0.25) dB in the wavelength range of 1440–1640 nm for the TE_0 (TM_0) mode and achieve minimal insertion loss as small as 0.08 (0.07) dB at the wavelength of 1550 nm. The cross talk maintains below −32 dB and −35 dB for the TE_0 and TM_0 modes, respectively. Experimentally, the fabricated waveguide crossing achieves measured insertion loss less than 0.20 (0.25) dB for the TE_0 (TM_0) mode with minimal insertion loss as small as 0.1 dB. The measured cross talk is below −28 dB and −31 dB for the TE_0 and TM_0 modes, respectively. Therefore, our proposed waveguide crossing can be widely applied in photonic integrated circuits to construct photonic systems with the capabilities of polarization control and mode (de)multiplexing.

https://doi.org/10.1364/OL.44.000077

Photonic systems are becoming more and more complicated, and the number of devices integrated on a single chip is also increasing exponentially. In a planar photonic circuit, waveguide crossings with negligible influence on the propagating light are indispensable. Many waveguide crossing designs have been investigated, such as multilayer structure crossing [1,2], photonic crystal waveguide crossing [3–5], multimode interference (MMI) crossing [6–12], and inverse-designed crossing [4,13,14]. Some of these demonstrated waveguide crossings have already shown negligible insertion loss and cross talk. Complex photonic systems usually need to control and process light with different polarizations, so waveguide crossings, which can transport light perfectly for different polarizations, are highly desired. MMI waveguide crossings [15] were demonstrated with polarization insensitivity. However, the insertion loss for both the TE_0 and TM_0 modes is relatively large. Subwavelength-grating polarization-insensitive waveguide crossings can achieve extremely low insertion loss, but the taper connecting the wire and subwavelength waveguides introduces large insertion loss and occupies a footprint of tens of square micrometers [16]. Therefore, a polarization-insensitive waveguide crossing connecting wire waveguides with compact sizes and negligible insertion loss and cross talk is yet to be realized.

Photonic inverse design is a generic and robust design method, which explores the full parameter space of device structures. In this Letter, we propose a low-loss and wideband polarization-insensitive waveguide crossing by using an inverse design method. The simulated insertion loss and cross talk maintain less than 0.18 (0.25) dB and −32 (−35) dB in the wavelength range of 1440–1640 nm with the values reaching 0.08 (0.07) dB and −37 (−38) dB, respectively, at the wavelength of 1550 nm for the TE_0 (TM_0) mode. Experimentally, the fabricated waveguide crossing maintains low insertion loss less than 0.20 dB (TE_0 mode) and 0.25 dB (TM_0 mode), and the cross talk maintains less than −28 dB (TE_0 mode) and −31 dB (TM_0 mode) in the wavelength range of 1440–1640 nm. At the wavelength of 1550 nm, the insertion loss and cross talk can reach as small as 0.10 (0.10) dB and −35 (−32) dB for the TE_0 (TM_0) mode.

The devices were designed on a silicon-on-insulator (SOI) wafer with a 250-nm-thick silicon layer embedded inside silicon oxide. Figure 1(a) shows the direct waveguide crossing, where the purple and gray regions denote silicon and silicon oxide, respectively. Figure 1(b) is a conceptual illustration of our proposed waveguide crossing. We take the waveguide crossing structure shown in Fig. 1(c) as an example to illustrate the design process. The design optimization region is restricted within a circle of 3 μm radius denoted by the blue line. Four continuous lines are used to delineate the borders of the waveguide crossing, and these lines are fitted from the discrete green dots by the triple spline interpolation. The position of each discrete dot is described by the radial and angular coordinates (r_i and θ_i). Due to the rotational symmetry, we only need to optimize 1/8 of the entire structure, as shown in Fig. 1(c). During the optimization, the black dots, which

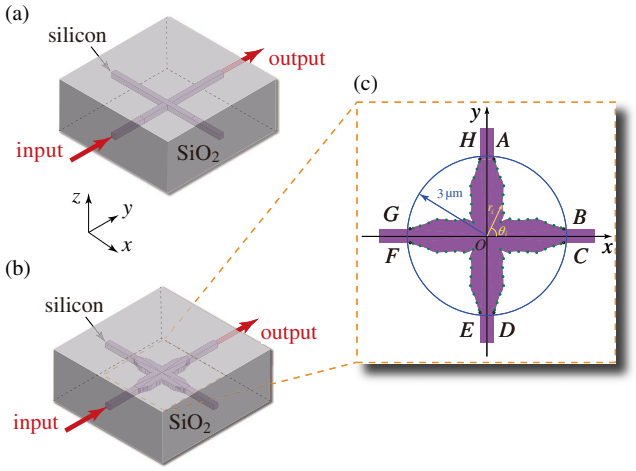

Fig. 1. Conventional and new schemes for directing light flow across a waveguide crossing on a chip. (a) Schematic of the direct waveguide crossing. The purple and gray regions represent Si and SiO_2, respectively. (b) Schematic of the inverse-designed waveguide crossing. (c) Top view of the inverse-designed waveguide crossing, the borders of which are defined by four continuous lines *AB*, *CD*, *EF*, and *GH* going through the green dots.

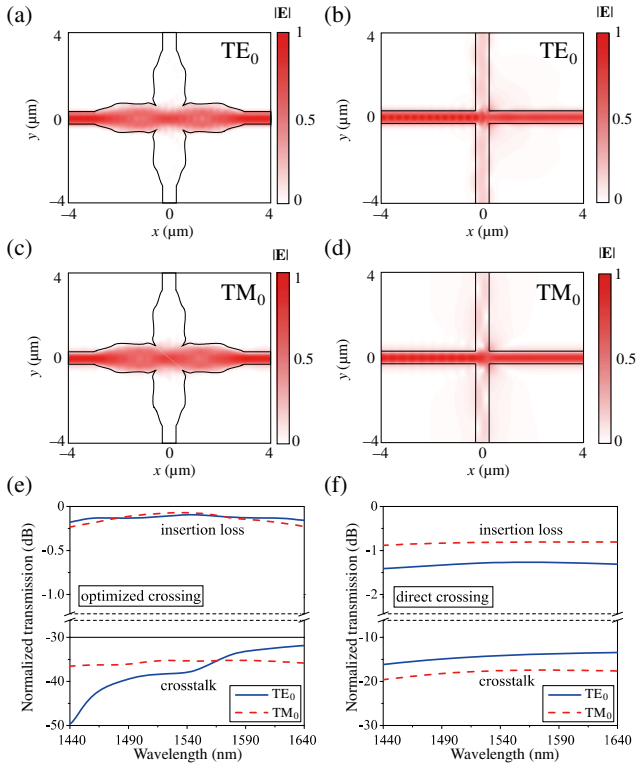

Fig. 2. (a), (b) Simulated electric field profiles of the TE_0 mode at 1550 nm transmitting through the (a) optimized and (b) direct waveguide crossing. (c), (d) Simulated electric field profiles of the TM_0 mode at 1550 nm transmitting through the (c) optimized and (d) direct waveguide crossing. (e), (f) Normalized insertion loss and cross talk spectra of the (e) optimized and (f) direct waveguide crossing for the TE_0 (blue solid lines) and TM_0 (red dashed lines) modes.

are used for connecting the waveguides, were fixed. The angular coordinates θ_i of the discrete dots were also fixed. The greedy optimization method was adopted to determine the radial coordinates r_i of the discrete dots. We first generated a random value for each dot, then optimized them in series. During the serial optimization, we varied the individual r_i and restricted the dot within the blue circle, while fixing all the other dots. The best r_i's were obtained after comparing the structural transmission of all attempted values. After several rounds of r_i optimization from the first dot to the last, the process was stopped when the insertion loss of both the TE_0 and TM_0 modes at 1550 nm could not be reduced in additional optimization runs. Based on the structure obtained from the greedy optimization method, we subsequently adopted a random-walk method to further improve the performance of the waveguide crossing. The radii r_i's of all dots were given a slight random variation. If the resulting insertion loss reduced, the change was accepted; otherwise, the change was discarded. This process was stopped when the insertion loss was below 0.1 dB. After ~48 h of optimization by using a normal 16-core desktop computer, we obtained the final design of the polarization-insensitive waveguide crossing, as shown in Fig. 1(c).

Figures 2(a) and 2(c) show the simulated electric field $|\mathbf{E}|$ profiles of the fundamental TE_0 and TM_0 modes, respectively, at 1550 nm transmitting through the optimized waveguide crossing. Figures 2(b) and 2(d) show the simulated electric field $|\mathbf{E}|$ profiles of the fundamental TE_0 and TM_0 modes, respectively, at 1550 nm transmitting through the direct waveguide crossing. It is clear that the optimized waveguide crossing has negligible influence on the light propagation compared with that of the direct waveguide crossing, which scatters a portion of the light into the cross waveguide. Figures 2(e) and 2(f) plot the normalized transmission spectra of the optimized and direct waveguide crossings. The insertion loss of the TE_0 (TM_0) mode can maintain less than 0.18 (0.25) dB in the wavelength range of 1440–1640 nm and reach as small as 0.08 (0.07) dB at the wavelength of 1550 nm. The cross talk of the optimized waveguide crossing maintains below −32 (−35) dB for the TE_0 (TM_0) mode. By contrast, the minimal insertion loss of the direct waveguide crossing is higher than 1.35 (0.84) dB, and the cross talk is higher than −16 (−19) dB for the TE_0 (TM_0) mode in the same wavelength range.

The waveguide crossing devices were fabricated on a SOI wafer with a 250-nm Si device layer on 3-μm buried oxide. The device patterns were defined along with the input and output waveguides and grating couplers in a single step of electron-beam lithography with ZEP520A resist. Then, the patterns were transferred to the top silicon layer by inductively coupled plasma reactive-ion etching with SF_6/C_4F_8 gas chemistry. Last, a 2.5-μm-thick silicon oxide layer was deposited on the top as an upper cladding by plasmon-enhanced chemical vapor deposition. Figures 3(a) and 3(b) are the optical microscope images of the fabricated devices for characterizing the insertion loss and cross talk of the optimized and direct waveguide crossings, respectively. We adopted on-chip grating couplers to couple light from an optical fiber into and out of the devices, because grating couplers can work not only as power couplers but also as mode selectors to couple light with the desired polarization into and out of the devices. Devices composed of a pair of grating couplers connected by a straight waveguide were used to extract the insertion loss and cross talk without waveguide crossings. We cascaded multiple optimized waveguide crossings in a

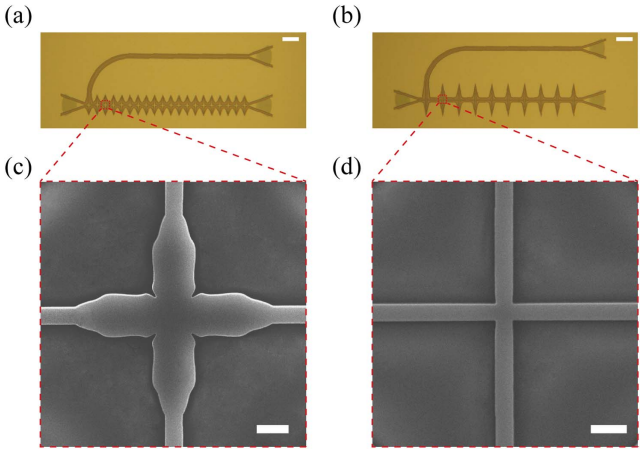

Fig. 3. (a), (b) Optical microscope images of the fabricated (a) optimized and (b) direct waveguide crossing. (c), (d) Scanning electron microscope (SEM) images of the fabricated (c) optimized and (d) direct waveguide crossing. The scale bars represent 20 μm in (a) and (b), and 1 μm in (c) and (d).

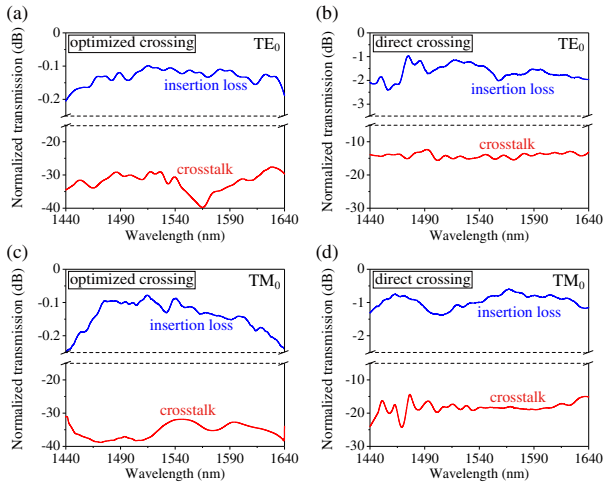

Fig. 4. (a), (b) Experimental insertion loss (blue lines) and cross talk (red lines) spectra of the (a) optimized and (b) direct waveguide crossing for the TE_0 mode. (c), (d) Experimental insertion loss (blue lines) and cross talk (red lines) spectra of the (c) optimized and (d) direct waveguide crossing for the TM_0 mode.

single device in order to measure the small insertion loss. Figures 3(c) and 3(d) are the SEM images, which are zoomed in at the optimized and direct waveguide crossings, respectively.

We characterized the fabricated devices by spectroscopic measurement of their optical transmission. A tunable semiconductor laser was used to measure the wavelength-dependent properties of the waveguide crossings in the wavelength range of 1440–1640 nm. The light was sent over a single-mode fiber with its polarization state adjusted by a fiber polarization controller and then coupled into the device under test via the input grating coupler. A photodetector was used to collect the light coupled out of the output grating coupler. For the TE_0 mode, the normalized transmission spectra measured from the through and cross ports of the optimized and direct waveguide crossings are plotted in Figs. 4(a) and 4(b), respectively. The measured insertion loss and cross talk of the optimized waveguide crossing maintain below 0.20 dB and −28 dB in the wavelength range of 1440–1640 nm. As a comparison, the insertion loss and cross talk of the direct waveguide crossing are higher than 1.00 dB and −16 dB in the same wavelength range. For the TM_0 mode, the normalized transmission spectra measured from the through and cross ports of the optimized and direct waveguide crossings are plotted in Figs. 4(c) and 4(d), respectively. The measured insertion loss and cross talk of the optimized waveguide crossing maintain below 0.25 dB and −31 dB in the wavelength range of 1440–1640 nm. As a comparison, the insertion loss and cross talk of the direct waveguide crossing are higher than 0.65 dB and −25 dB in the same wavelength range. Figure 5 plots the insertion loss of the optimized and direct waveguide crossings as a function of the number of crossings at the wavelength of 1550 nm for the TE_0 [Fig. 5(a)] and TM_0 [Fig. 5(b)] modes. The fitted lines indicate that the insertion loss of a single optimized and direct waveguide crossing is 0.10 (0.10) dB and 1.31 (0.85) dB, respectively, for the TE_0 (TM_0) mode. It should be noted that most of previous demonstrated waveguide crossings were designed for only one polarization and could not achieve low insertion loss for both the TE_0 and TM_0 modes simultaneously [7,10,11]. Although some waveguide crossings could work for both the TE_0 and TM_0 modes [15,16], our proposed crossing compares favorably with those structures. Ours has ∼30% (in dB) lower insertion loss than that in Ref. [15]. The crossing in Ref. [16] not only requires a 50-μm-long subwavelength grating, but also introduces 0.592 dB and 0.97 dB loss (mainly from the tapers) for the TE_0 and TM_0 modes, respectively.

Due to uncontrollable imperfection in nanofabrication, the sizes of fabricated devices can often have tens of nanometers deviation from the original design. Therefore, fabrication tolerance is an important characteristic for assessing the performance of devices. Here, we simulated the transmission of the optimized waveguide crossing with size variation of $\Delta w = \pm 40$ nm, as shown in Fig. 6(a), and the results are plotted in Figs. 6(b) and 6(c) for the TE_0 and TM_0 modes, respectively. The normalized transmission spectra of the ideal structure and the structures with $\Delta w = 40$ nm and −40 nm clearly indicate that the optimized waveguide crossing preserves similar performance under the size variation of $\Delta w = \pm 40$ nm.

In conclusion, we have designed a polarization-insensitive waveguide crossing with low insertion loss and low cross talk

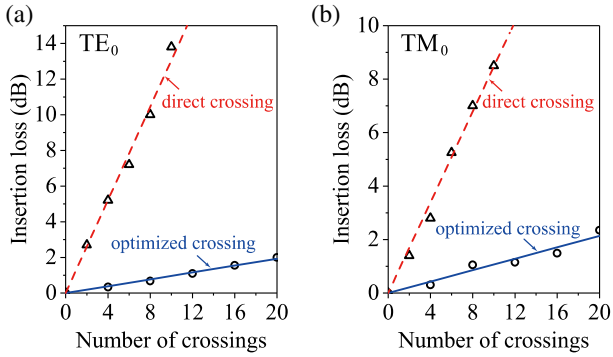

Fig. 5. Measured insertion loss of the optimized (blue solid lines) and direct (red dashed lines) waveguide crossing as a function of the number of crossings for the (a) TE_0 and (b) TM_0 modes.

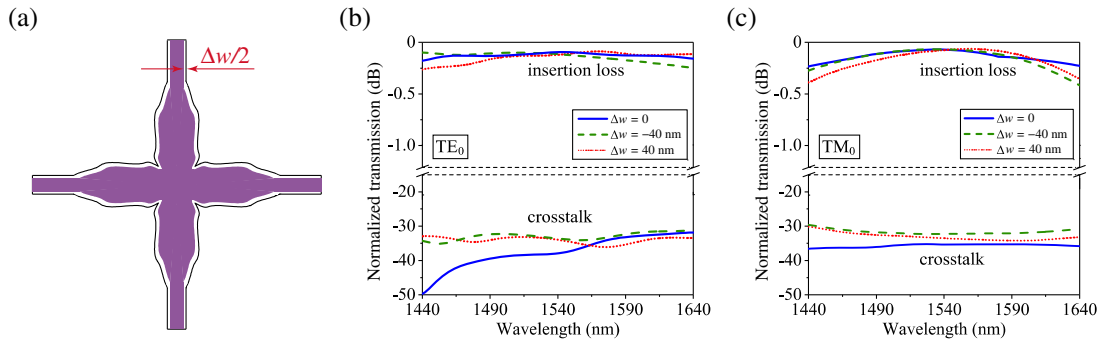

Fig. 6. (a) Illustration of a typical fabrication error of optimized waveguide crossing. The purple area denotes the fabricated structure, while the black solid line denotes the border of the original design. The width of the fabricated structure may have a deviation Δw from the designed value. (b), (c) Analysis of fabrication deviation in optimized waveguide crossing for the (b) TE_0 and (c) TM_0 modes. Blue solid, green dashed, and red dotted lines represent the ideal structure, the structure with width deviation $\Delta w = -40$ nm, and the structure with width deviation $\Delta w = 40$ nm, respectively.

by using an inverse design method and experimentally demonstrated its functionality on a chip. The fabrication process is simple and straightforward, which involves only a single step of electron-beam lithography, plasma dry etching, and silicon oxide deposition. From both simulated and experimental results, the insertion loss of the TE_0 and TM_0 modes maintains below 0.20 dB and 0.25 dB, respectively, and their cross talk maintains below −28 dB and −31 dB, respectively, in the wavelength range of 1440–1640 nm. At the wavelength of 1550 nm, the insertion loss and the cross talk can reach as small as 0.10 (0.10) dB and −35 (−32) dB for the TE_0 (TM_0) mode. Therefore, the inverse-designed and experimentally demonstrated waveguide crossings have great potential as a standard module in the silicon photonic integrated circuitry for constructing high-density photonic integrated networks.

Funding. Hong Kong Research Grants Council Early Career Scheme (24208915); Hong Kong Research Grants Council General Research Fund 14208717; National Natural Science Foundation of China (NSFC) and Research Grants Council of Hong Kong Joint Research Scheme (N_CUHK415/15).

†These authors contributed equally to this work.

REFERENCES

1. A. M. Jones, C. T. DeRose, A. L. Lentine, D. C. Trotter, A. L. Starbuck, and R. A. Norwood, Opt. Express **21**, 12002 (2013).
2. K. Shang, S. Pathak, B. Guan, G. Liu, and S. J. B. Yoo, Opt. Express **23**, 21334 (2015).
3. Y. Yu, M. Heuck, S. Ek, N. Kuznetsova, K. Yvind, and J. Mørk, Appl. Phys. Lett. **101**, 251113 (2012).
4. L. Lu, M. Zhang, F. Zhou, W. Chang, J. Tang, D. Li, X. Ren, Z. Pan, M. Cheng, and D. Liu, Opt. Express **25**, 18355 (2017).
5. M. M. Gilarlue, S. H. Badri, H. Rasooli Saghai, J. Nourinia, and C. Ghobadi, Photon. Nanostruct. **31**, 154 (2018).
6. Y. Zhang, S. Yang, A. E. J. Lim, G. Q. Lo, C. Galland, T. Baehr-Jones, and M. Hochberg, IEEE Photon. Technol. Lett. **25**, 422 (2013).
7. Y. Liu, J. M. Shainline, X. Zeng, and M. A. Popović, Opt. Lett. **39**, 335 (2014).
8. C. Sun, Y. Yu, and X. Zhang, Opt. Lett. **42**, 4913 (2017).
9. C. H. Chen and C. H. Chiu, IEEE J. Quantum Electron. **46**, 1656 (2010).
10. Y. Zhang, A. Hosseini, X. Xu, D. Kwong, and R. T. Chen, Opt. Lett. **38**, 3608 (2013).
11. Y. Ma, Y. Zhang, S. Yang, A. Novack, R. Ding, A. E.-J. Lim, G.-Q. Lo, T. Baehr-Jones, and M. Hochberg, Opt. Express **21**, 29374 (2013).
12. W. Bogaerts, P. Dumon, D. V. Thourhout, and R. Baets, Opt. Lett. **32**, 2801 (2007).
13. W. Chang, L. Lu, X. Ren, D. Li, Z. Pan, M. Cheng, D. Liu, and M. Zhang, Photon. Res. **6**, 660 (2018).
14. P. Sanchis, P. Villalba, F. Cuesta, A. Håkansson, A. Griol, J. V. Galán, A. Brimont, and J. Martí, Opt. Lett. **34**, 2760 (2009).
15. S.-H. Kim, G. Cong, H. Kawashima, T. Hasama, and H. Ishikawa, Opt. Express **22**, 2545 (2014).
16. P. J. Bock, P. Cheben, J. H. Schmid, J. Lapointe, A. Delâge, D.-X. Xu, S. Janz, A. Densmore, and T. J. Hall, Opt. Express **18**, 16146 (2010).